Translational Oncology 20 (2022) 101400

Contents lists available at ScienceDirect

Translational Oncology

journal homepage: www.elsevier.com/locate/tranon

Original Research

Force-feeding malignant mesothelioma stem-cell like with exosome-delivered miR-126 induces tumour cell killing

Federica Monaco [a,e], Laura De Conti [b], Simone Vodret [c], Nunzia Zanotta [d], Manola Comar [d], Sandra Manzotti [a], Corrado Rubini [e], Laura Graciotti [e], Gianluca Fulgenzi [a], Massimo Bovenzi [f], Marco Baralle [b], Marco Tomasetti [a,*], Lory Santarelli [a]

[a] Department of Clinical and Molecular Sciences, Polytechnic University of Marche, Ancona, Italy
[b] RNA biology Group, International Centre for Genetic Engineering and Biotechnology (ICGEB), Trieste, Italy
[c] Cardiovascular Biology Laboratory, International Centre for Genetic Engineering and Biotechnology (ICGEB), Trieste, Italy
[d] Institute for Maternal and Child Health - IRCCS "Burlo Garofolo", Trieste, Italy
[e] Department of Excellence SBSP-Biomedical Sciences and Public Health, Polytechnic University of Marche, Ancona, Italy
[f] Department of Medical Sciences, Clinical Unit of Occupational Medicine, University of Trieste, Trieste, Italy

ARTICLE INFO

Keywords:
Mesothelioma
miR-126
exosome
spheroids
miRNA-based therapy

ABSTRACT

Malignant pleural mesothelioma (MPM) is an aggressive tumour resistant to treatments. It has been postulated that cancer stem cells (CSCs) persist in tumours causing relapse after multimodality treatment. In the present study, a novel miRNA-based therapy approach is proposed. MPM-derived spheroids have been treated with exosome-delivered miR-126 (exo-miR) and evaluated for their anticancer effect. The exo-miR treatment increased MPM stem-cell like stemness and inhibited cell proliferation. However, at a prolonged time, the up taken miR-126 was released by the cells themselves through exosomes; the inhibition of exosome release by an exosome release inhibitor GW4869 induced miR-126 intracellular accumulation leading to massive cell death and in vivo tumour growth arrest. Autophagy is involved in these processes; miR-126 accumulation induced a protective autophagy and the inhibition of this process by GW4869 generates a metabolic crisis that promotes necroptosis, which was associated with PARP-1 over-expression and cyt-c and AIF release. Here, for the first time, we proposed a therapy against CSCs, a heterogeneous cell population involved in cancer development and relapse.

Introduction

Malignant pleural mesothelioma (MPM) is an aggressive, rare tumour, with few therapeutic options [1, 2]. New strategies that lead to more efficient and proficient handling of MPM are needed. Studies have shown that miR-126 can act as a tumour suppressor in MPM through direct modulation of downstream target IRS1 [3–5]. However, the in vivo delivery of miRNAs faces various obstacles due to their poor biological stability, short half-life, poor oral bioavailability, inappropriate intracellular release properties and other unfavourable factors [6,7]. Therefore, developing effective miRNA delivery approaches are necessary for successful miRNA-based therapy. Recently, due to the intrinsic molecular characteristics such as high editability and low immunogenicity, extracellular vesicles (EVs) have been proposed as the most suitable candidate [8]. Exosomes are a type of EVs, which are released by all cell types to mediate cell-to-cell communication both at the paracrine and the systemic levels, suggesting a role for them as an ideal nano-delivery system. The anticancer effect of miR-126 using HUVEC-derived exosomes as a delivery system was previously evaluated in an in vitro stromal model. All cellular components of the 'stroma' took up exo-miR-126 in a dose- and time-dependant manner and released exosomes enriched in miR-126 into the microenvironment, reducing angiogenesis and tumour growth [9].

Tumours may often originate from the transformation of normal stem cells, and cancer cells may include subpopulations of CSCs. There is now evidence that CSCs play a role in the development and growth of most human malignancies and cancer cell repopulation can be attributed to CSCs due to their ability to escape immune surveillance and higher resistance to conventional therapy [10, 11]. Therefore, specific targeting of CSCs may improve the efficiency of cancer therapy. In the present study, we developed a new method for MPM treatment. MPM

* Corresponding author at: via Tronto 10A, 60126, Italy.
E-mail address: m.tomasetti@univpm.it (M. Tomasetti).

https://doi.org/10.1016/j.tranon.2022.101400
Received 8 March 2022; Accepted 11 March 2022
Available online 23 March 2022
1936-5233/© 2022 The Authors. Published by Elsevier Inc. This is an open access article under the CC BY-NC-ND license (http://creativecommons.org/licenses/by-nc-nd/4.0/).

Abbreviations

3-ABA	3-aminobenzamide
Adh	adherent cells
AIF	apoptosis-inducing factor
AMPK	AMP-activated protein kinase
BAX	BCL2 associated X
BID	BH3-interacting domain death agonist
CD31	cluster of differentiation 31
CSCs	cancer stem cells;
cyt-c	cytochrome-c
cyto	cytoplasm
exo-miR	exosome-delivered miR-126 EGF, epidermal growth factor
EGFL7	epidermal growth factor like domain 7
EVs	extracellular vesicles
FBS	foetal bovine serum
bFGF	basic fibroblast growth factor
FFPE	formalin-fixed paraffin-embedded tissue
GAPDH	glyceraldehyde-3-phosphate dehydrogenase
GW	GW4869
H&E	haematoxylin and eosin
HRP	horseradish peroxidase
HUVEC	human umbilical vein endothelial cells
IgG	immunoglobulin G
IHC	immunohistochemical
IRS1	insulin receptor substrate 1
IL	interleukin
KLF4	kruppel like factor 4
LC3	microtubule-associated protein 1A/1B-light chain 3
LVES	large vessel endothelial supplement
MPM	malignant pleural mesothelioma
mTOR	mammalian target of rapamycin
OCT4	octamer-binding transcription factor 4
OD	optical density
org	organelle
p70S6K	ribosomal protein S6 kinase beta-1
PARP-1	poly [ADP-ribose] polymerase 1
PI	propidium iodide
RT	reverse transcription
RT	room temperature
SD	standard deviation
SEM	standard error of the mean
SOX2	SRY-box transcription factor 2
Sph	spheroids
TEM	Transmission electron microscopy
ULK1	unc-51-like kinase 1
VEGF	vascular endothelial growth factor

stem-cells like were treated with miR-126-enriched exosome after a pre-treatment with an inhibitor of exosome release, thereby forcing miR-126 within the cancer cells leading to massive cell death.

Materials and methods

Cell culture

Met-5A (mesothelial cells), H28 (MPM sarcomatoid cells) and MSTO-211H (MPM biphasic cells), from ATCC, were grown in RPMI medium supplemented with 10% foetal bovine serum (FBS), 1% penicillin and 1% streptomycin (all Life Technologies), while MPP89 (MPM epithelial cells) were maintained in Ham's F10 with 15% FBS and supplemented with glutamine (2 mM) and antibiotics. The HUVECs obtained from Gibco (Life Technologies) were grown in Medium 200 (Life Technologies) with large vessel endothelial supplement (LVES; Life Technologies). All cells were cultured in a humidified incubator at 37 °C and in an atmosphere of 5% CO_2. The cells were periodically checked for the absence of mycoplasma contamination using the PCR mycoplasma test. Cell authentication was performed using a PowerPlex Fusion 6C system (Promega, Fitchburg, WI).

Spheroid formation

Three-dimensional spheroids with cancer stem cell-like properties were obtained by culturing MSTO-211H and MPP89 cell lines in ultra-low attachment 24-well or 96-well plates (Corning Life Sciences) at a density of 10^4 cells/ml in serum-free DMEM-F12 (Euroclone) supplemented with 1 × B27 (Invitrogen), 20 ng/ml basic fibroblast growth factor (bFGF; Millipore), 20 ng/ml epidermal growth factor (EGF; Sigma). The plates were incubated at 37 °C in a humidified atmosphere of 5% CO_2. Fresh medium was replaced every 3 days and after 10-day incubation, spheroids of 100–200 μm diameter were formed. Spheroid formation was monitored using a Leica microscope (Leitz, Inc.) at 10X magnification and with a Spot Insight 3.2.0 camera with Spot Advanced software (Spot Imaging).

Exosome isolation and uptake

Exosomes were isolated from HUVEC transiently transfected with miR-126 mimic (exo-miR, 100 nM, MISSION microRNA Mimic, Sigma) and miRNA mimic scrambled control (exo-scr, 100 nM, MISSION microRNA Mimic Negative Control 2, Sigma) or antisense miR-126 (exo-antimiR, 50 nM, MISSION microRNA Inhibitor, Sigma) in exosome-depleted serum-containing medium using High Perfect Transfection reagent (Qiagen) according to the manufacturer's instructions. After 72 h of incubation, exosomes were obtained and purified using differential centrifugations as previously described [9]. After isolation, the pellet was re-suspended in PBS, treated with 0.1 mg/ml RNase A (Qiagen) for 30 min at 37 °C to remove miRNA contamination, and clarified using a 0.22 μm filter before use. After treatment and filtration, the protein content of the purified exosomes was measured using the Bradford assay (Sigma). All ultracentrifugation steps were performed at 4 °C in a Beckton Dickinson ultracentrifuge fitted with the TLS-55 swing bucket rotor.

The exosome uptake was assessed by labelling exosomes with the green fluorescence plasma membrane stain PKH67 (exo-PKH67, 20 μM; Sigma). Spheroids were cultured in a 96-well plate, and PKH67-labelled exosomes (20 μg/ml) were added to the exosome-depleted culture medium. After 24 h of incubation, the spheroids were seeded on coverslips using a cytospin 2 centrifuge (Shandon), and exosome uptake was assessed by AxioCam MRc5 fluorescent microscope (Zeiss Imager A1).

Treatments

Non-malignant mesothelial (Met-5A), MPM cell lines and the MPM-derived spheroids were treated with exo-miR, exo-scr or exo-antimiR (20 μg/ml) with and without a pre-treatment (24 h) with the inhibitor of exosome secretion GW4869 (20 μM in DMSO). The PARP-1 inhibitor 3-aminobenzamide (3-ABA) was added to the culture medium 2 h before treatments at 2 mM. A solution of 1% DMSO (Sigma-Aldrich) was used as a negative control.

Detection of cell death and proliferation

Apoptosis detection: Apoptosis was quantified using the annexin V-FITC and propidium iodide (PI) methods. Briefly, adherent cells (10^5 cells/ml) or spheroids (10^4cells/ml) were plated in 12-well or 24-well plates, respectively. After an overnight incubation, cells were treated with exo-miR or exo-scr with and without a pre-treatment (24 h) with GW4869 (20 μM). After 48 h of treatment, floating and attached cells were collected, washed twice with PBS, resuspended in 0.1 ml binding buffer (10 mM HEPES, 140 mM NaCl, 5 mM CaCl2, pH 7.4), incubated for 20 min at room temperature with 2 μl annexin V-FITC, supplemented with 10 μl of PI (10 μg/ml), and analysed by flow cytometry (Becton Dickinson, Rutherford, NJ, USA). Alternatively, PI staining was evaluated by AxioCam MRc5 fluorescent microscope (Zeiss Imager A1).

Cell proliferation assay: Cells were incubated with a solution of crystal violet (0.2% and 2% of ethanol in water) at 37 °C for 5 min. After removing the media, 200 μl of isopropanol was added to dissolve the crystals, and the absorbence read at 570 nm in an ELISA plate reader (Tecan).

Immunohistochemistry

Formalin-fixed paraffin-embedded tissue (FFPE) sections of the tumours, and spheroids were cut at 2.5-μm thickness, unmasked, and deparaffinised in citrate buffer (10 mM, pH 6.0) at 98 °C for 15 min. After blocking, the tumour sections were incubated with anti-Ki67 (Dako), anti-VEGF (Santa Cruz Biotechnology, USA), and anti-CD31 (Dako) at 4 °C overnight and then, automated IHC was performed on Omnis platform (Agilent, USA). The FFPE sections of the liver, lung and kidney were deparaffinised and stained for haematoxylin and eosin for histological evaluation. The sections were inspected in an optic microscope (Axiocam MRc5, Zeiss).

Quantitative RT-PCR

Total cellular RNA was obtained using an RNeasy Mini Kit (Qiagen) according to the manufacturer's instructions. First-strand cDNAs were synthesized from the mRNAs by individual TaqMan miRNA Assay (Applied Biosystems, Life Technologies) using a High-Capacity cDNA Reverse Transcription Kit (Life Technologies) according to the manufacturer's instructions.

MiR-126 was directly detected in adherent cells and spheroids according to Too et al [12]. Briefly, cells (10^3–10^4) were lysed in a lysis solution containing triton-X (2%), NP40 (2%), DNase (2 μl) in a total volume of 40 μl. After incubation at 37 °C for 30 min and at 70 °C for 10 min, 5 μl of cell lysate were added to 10 μl of RT reagents.

Circulating miR-126 was detected in serum samples as described previously [13]. Haemolyzed serum samples from mice were excluded from the analysis. Solubilize proteins were deactivated by mixing 2.5 μL of serum sample with 2.5 μL of a preparation buffer containing 2.5% Tween 20 (Euroclone), 50 mmol/L Tris (Sigma-Aldrich), and 1 mmol/L EDTA (Sigma-Aldrich). Then, 5 μl of RT reagent mixture were directly added to 5 μL of serum in preparation buffer: 2 h incubation at 37 °C was followed by a 5 min enzyme inactivation at 95 °C. The transcribed cDNA was then centrifuged at 9000 g for 5 min to eliminate the protein precipitant.

A 1.33 μL volume of the supernatant cDNA solution was used as the template for qPCR. The qPCR conditions were 60 °C for 2 min, 95 °C for 10 min, in 40 cycles of 95 °C for 15 s and 60 °C for 1 min. The qRT-PCR reactions performed in duplicate were carried out using a TaqMan® Fast Advanced Master gene expression kit (Applied Biosystems, Life Technologies) and U6 for normalization.

The SOX2, OCT4, NANOG, KLF4, c-MYC, IRS1, VEGF, EGFL7, IL-6 and IL-1 first-strand cDNA was synthesized using a High-Capacity cDNA Reverse Transcription Kit (Life Technologies). The qRT-PCR was performed using SYBR Select Master Mix (Life Technologies) with GAPDH as a housekeeping gene.

Transmission electron microscopy (TEM)

Spheroids from MSTO-211H were plated in 96-well plates at 1×10^3 per well. After treatment with the drugs as mentioned above, the cells were harvested, overnight fixed in 2.5% glutaraldehyde at 4 °C, and centrifuged to form pellets. The pellets were post-fixed in 0.5% osmium tetroxide for 30 min at room temperature (RT), embedded in agarose low-melting (3%), dehydrated in acetone, and embedded in an Epoxy-Araldite mixture (Epoxy-Embedding kit, Sigma). Thin sections were obtained with a Reichert Ultratome (Reichert Technologies, Depew, NY, USA), stained with lead citrate, and examined using the Philips CM 10 transmission electron microscope (Philips, Eindhoven, The Netherlands).

Western blot analysis

Spheroids with and without treatments (24 h) were lysed in RIPA buffer containing Na_3VO_4 (1 mM) and protease inhibitors (1 μg/ml). For subcellular fractionation, spheroids (in 24-well plates) were treated with GW-exo-miR for 24 h, harvested, and the pellet re-suspended in the digitonin cell permeabilization buffer (Trevigen, Gaithersburg, MD). The supernatant containing the cytosolic fraction was collected. The remaining pellet (organelle fraction) was lysed in the RIPA buffer containing Na_3VO_4 (1 mM) and protease inhibitors (1 μg/ml). Protein concentration was assessed by the Bradford assay. The lysates (10 μg of protein) were separated using 4–12% SDS-PAGE (Life Technologies) and transferred onto a nitrocellulose membrane (Protran). After blocking with 5% non-fat milk in PBS-Tween (0.1%), the membranes were incubated overnight at 4 °C with primary antibodies against LC3B, phospho-mTOR (p-mTOR$^{ser\text{-}2448}$), mTOR, phospho-p70S6K$^{ser\text{-}235/236}$, p70S6K, PARP-1, BID, BAX, Caspase-8, Caspase-9, Caspase-3, cyt-c, AIF, pAMPK$^{thr\text{-}172}$, AMPK, pULK1$^{ser\text{-}555}$ and ULK1 (all Cell signaling). β-Actin or GAPDH (Cell Signalling) was used as a loading control. After incubation with HRP-conjugated secondary IgG (Cell Signalling), the blots were developed using ECL (Pierce). The band intensities were visualized and quantified with ChemiDoc using Quantity One software (Bio-Rad Laboratories).

Animal study

All animal ethical and experimental procedures were evaluated and approved by the ICGEB Animal Welfare Board and the Italian Ministry of Health (Ministero Italiano della Salute, authorization no. 319/2020-PR), in full respect of the EU Directive 2010/63/EU.

Male NSG (NOD *SCID* gamma) mice (Jackson Laboratory, stock no. 005,557) were maintained in individually ventilated cages in a temperature-controlled environment with 12-hour light/dark cycles and received a standard chow diet and water ad libitum at the ICGEB animal Bio-experimentation facility. At 8 weeks of age, 1.5×10^6 MSTO-211H cells were injected at the dorsal subcutaneous level. After 10 days from MSTO-211H inoculation, when all masses were clearly detectable, mice were intra-tumour (i.t.) treated with: PBS (CTRL group), scramble exosomes (0.7 mg/Kg) (exo-scr group), miR-126-enriched exosomes (0.7 mg/Kg) (exo-miR group), alone or combined with an intra-tumour pre-treatment **(6 h)** with GW4869 (1 mg/Kg) (GW group, GW-exo-scr group and GW-exo-miR group). Treatments were performed on days 10, 13 and 16 upon tumour cell inoculation. Tumour size and body weight were measured every 3 days from day 10 to day 30 after MSTO-211H cell inoculation. The tumour volume was quantified by calliper and analysed using the formula: tumour volume (mm^3) = (d^2 * D)/2, where d and D, are the shortest and longest diameter in mm, respectively and the relative tumour growth rate was expressed as a percentage of final tumour volume/initial tumour volume ratio [14].

Statistical analysis

Data are presented as means ± standard deviations (SDs) or standard error of mean (SEM). Comparisons between groups of data were determined using Student's *t*-test. Multiple comparisons were performed by one-way analysis of variance (ANOVA) or ANOVA repeated measure with Tukey's post hoc analysis. A p-value ≤ 0.05 indicated statistical significance. All statistical analyses were performed using SPSS software.

Results

Spheroid formation, miR-126-enriched exosomes uptake and cytotoxic effect

Differently to H28 cells, which did not form spheroids (data not shown), both MSTO-211H and MPP89 form spheroids with cancer stem cell-like properties, showing increased expression of stemness markers such as SOX2, OCT4, NANOG, KLF4, and c-MYC with respect to their adherent cell counterparts. The treatment of MPM stem cells like with miR-126-enriched exosomes (exo-miR) further increased the expression of the stemness gene c-MYC in MISTO 211H cells and of stemness genes SOX2, OCT4, NANOG, KLF4 in MPP89 cells, thus inducing pluripotency in these cells (**Fig. S1**).

The spheroids from MSTO-211H and MPP89 cells internalized the exosomes, as visualized by punctuate green fluorescence (**Fig. 1A**). The exosome uptake was associated with significant reductions in MPM cell growth in 3-D spheroid models in both MSTO-211H and MPP89 as shown by the reduction of spheroid volume (spheroid diameter) and mass disaggregation found in MSTO-211H after 48-hours of exo-miR treatment (Fig. 1B). Reduction in Ki67 positive cells was also observed in both MSTO-211H and MPP89-derived spheroids (Fig. 1C).

As previously observed [9], the exo-miR treatment resulted in an intracellular reduction of miR-126 with respect to untreated cells (**Fig. S1**); as previously shown the MPM cells secreted miR-126 via exosomes to rid its cancer-killing effects. The exosomes enriched in

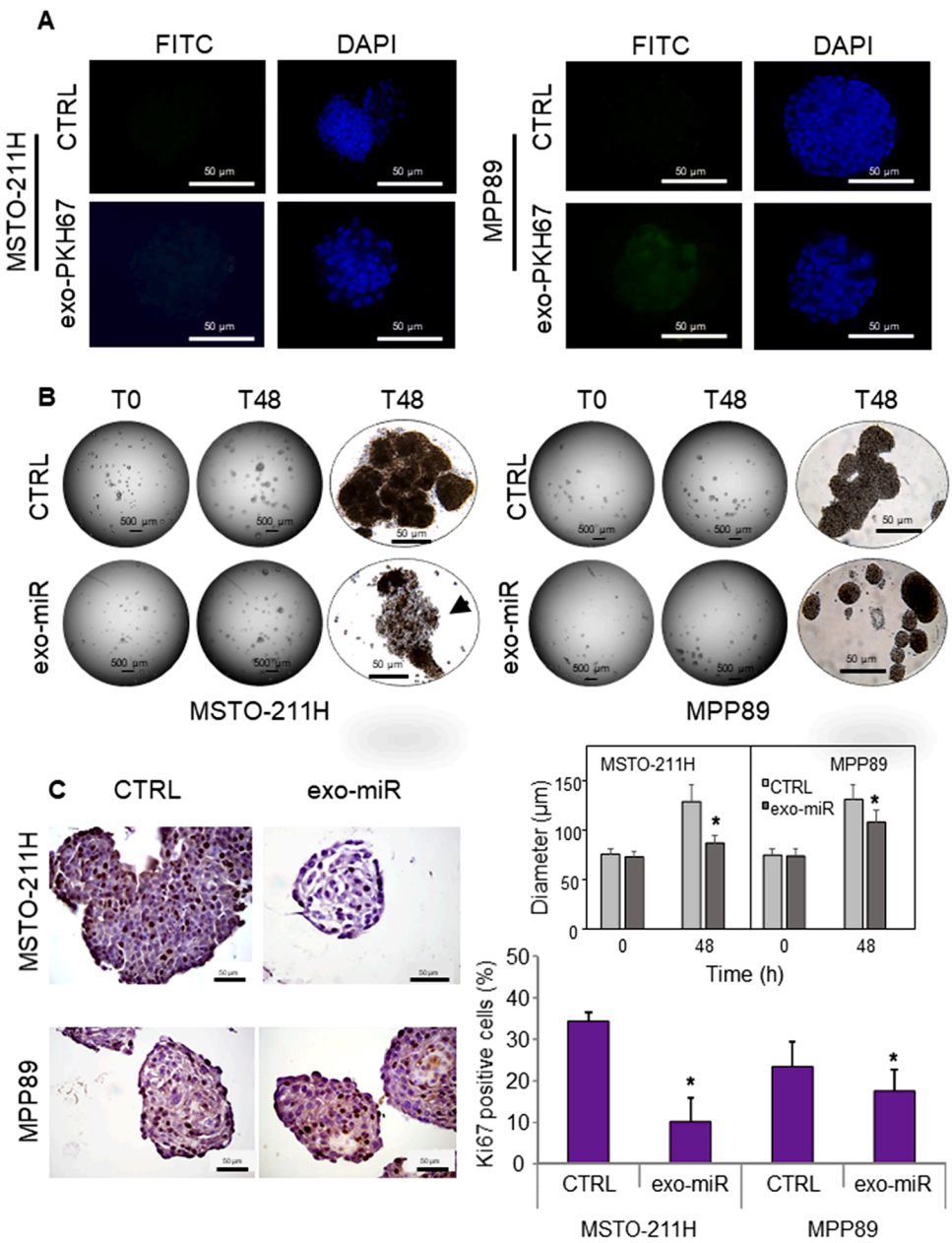

Fig. 1. Exosome uptake and cytotoxicity in spheroids. **A**) Spheroids from MSTO-211H and MPP89 were treated with PKH67-labelled exosomes (exo-PKH67, 20 µg/ml) for 24 h, and exosome internalization was visualized by fluorescence microscopy (Zeiss, AxioCam MRc5). **B**) Cancer stem cell-like MSTO-211H (left panel) and MPP89 (right panel) in spheroids (phase contrast images, 2.5X and 10X magnification) were treated with exo-miR (20 µg/ml) and growth and cytotoxicity evaluated before (T0) and after 48 h of incubation (T48) as spheroid size (diameter) and morphological changes. **C**) Cell proliferation evaluated as Ki67-positive cells after 24 h of incubation with exo-miR, the right panel shows quantification. Diameter quantification was performed by using ImageJ software. The scale bars indicate 50 µm and 500 µm. The images are representative of three independent experiments performed in duplicate and the data shown are mean values ± SD. Comparisons between groups were determined by Student's *t*-test. The symbol '*' denotes statistically significant differences between untreated cells (CTRL) and exo-miR-treated cells, $p < 0.05$.

miR-126 were released into cancer stroma, which may be internalized by the cells themselves or other cellular components of the environment. Therefore, we aimed to increase miR-126 intracellular level by inhibiting exosome secretion. The hypothesis being that if exosome secretion were significantly inhibited, that miR-126 stores within tumour cells and lead to oncogenic targeting and subsequent cell death. Incubation of MPM-derived spheroids with the inhibitor of exosome secretion GW4869 (GW, 20 μM) for 24 h, resulted in a significant increase of intracellular miR-126 in both exo-miR treated MSTO-211H and MPP89-derived spheroids (Fig. 2**A, B**). The GW treatment induced spheroids to attach to the plate, and when combined with exo-miR induced significant amounts of cell death as observed by phase-contrast imaging and PI cytotoxicity assay in MSTO-211H-derived spheroids (Fig. 2**C**). As well, an increased number of PI-positive cells, a sign of cell death, was also found in MPP89-derived spheroids after 48 h of treatment with exo-miR and GW (Fig. 2**D**).

To validate our hypothesis regarding retention of exosomes and cell death, we assessed the type of cell death induced by force-feeding the

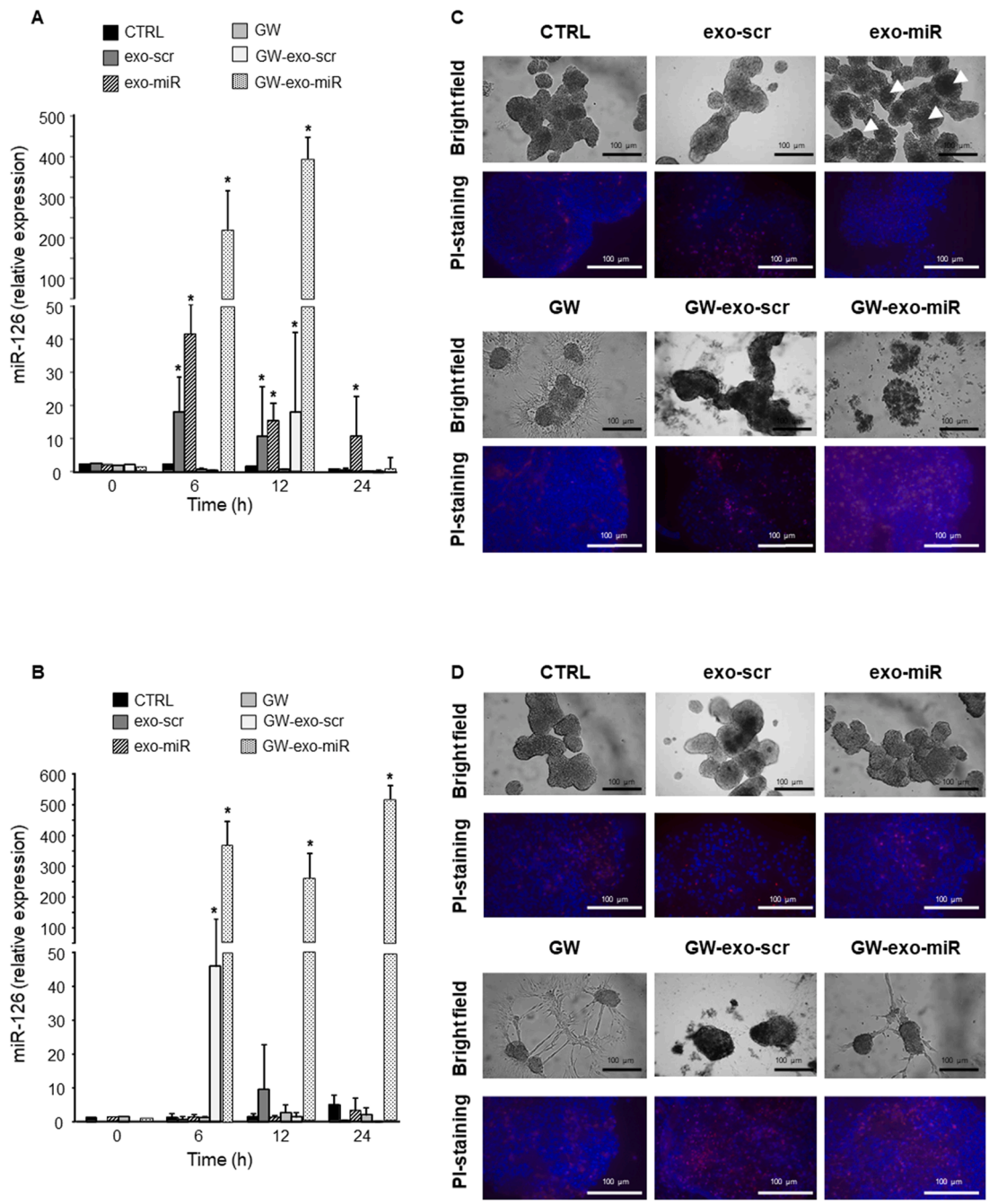

Fig. 2. MiR-126 level and cytotoxicity in spheroids after combined treatments. Spheroids from MSTO-211H and MPP89 were treated with exosome scramble (exo-scr), miR-126-enriched exosome (exo-miR), GW4869 (GW), GW4869 plus exosome scramble (GW-exo-scr), and GW4869 plus miR-126-enriched exosome (GW-exo-miR) and the expression of miR-126 over time was evaluated in MSTO-211H (**A**) and MPP89 (**B**) cancer stem cell-like. The cytotoxicity was evaluated after 48 h of incubation in MSTO-211H (**C**) and MPP89 (**D**) cancer stem cell-like as morphological changes (bright field) and PI staining evaluated by AxioCam MRc5 optic and fluorescent microscope (Zeiss Imager A1), respectively. The images are representative of four independent experiments performed in duplicate and the data shown are mean values ± SD. The scale bar indicates 100 μm. Comparisons amongst groups ($n = 4$) were determined by one-way ANOVA with Tukey post-hoc analysis. The symbol '*' denotes statistically significant differences amongst untreated cells (CTRL) and treated cells, $p < 0.05$.

MPM-derived spheroids with miR-126 delivered by exosomes. Three major types of morphologically distinct cell death: apoptosis (type I cell death), autophagic cell death (type II), and necrosis (type III) were evaluated in spheroids treated with exo-scr, exo-miR with and without pre-treatment with GW. The GW or exo-miR alone induced cell death mainly by a necrotic process, while an increase of late apoptosis was found in GW and exo-miR combination (**Fig. 3-left panel**). Necrosis occurs at the late stage of apoptosis or autophagy through distinct and sometimes overlapping, signalling pathways that are engaged in response to specific stimuli. The stemness phenotype enhanced the GW plus exo-miR-induced cell death; the treatment increased the expression of the stemness-related genes (**Fig. 3-right panel**).

The necrotic/apoptotic (necroptosis) effect was less pronounced by force-feeding adherent MPM cells (H28, MSTO-211H and MPP89) with miR-126-enriched exosomes; the accumulation of miR-126 within cells mostly inhibited cell proliferation rather than induced cell death (**Fig. S2**).

In vivo study

The inhibitory effect of MSTO-211H cell growth by the treatments was also evaluated in vivo by the xenograft SCID mice model (**Fig. 4A**). After tumour formation (10 days, tumour volume 25.5 ± 16.4 mm^2), mice were intra-tumoral (i.t.) treated with PBS ($n = 8$), exo-scr ($n = 10$) and exo-miR ($n = 10$) alone or after an intra-tumoral pre-treatment (6 h) with GW4869 ($n = 10$ each) at day 10, 13 and 16. Tumour volume and mouse body weight were checked every three days for 20 days.

As shown in **Fig. 4B**, the kinetics of tumour growth were or was significantly inhibited by the GW and exo-miR combination. The administration of exo-miR i.t. significantly inhibited the tumour growth (27%), which was further inhibited when was combined with GW (70%). An inhibitory effect was also observed for GW and exo-scr i.t.

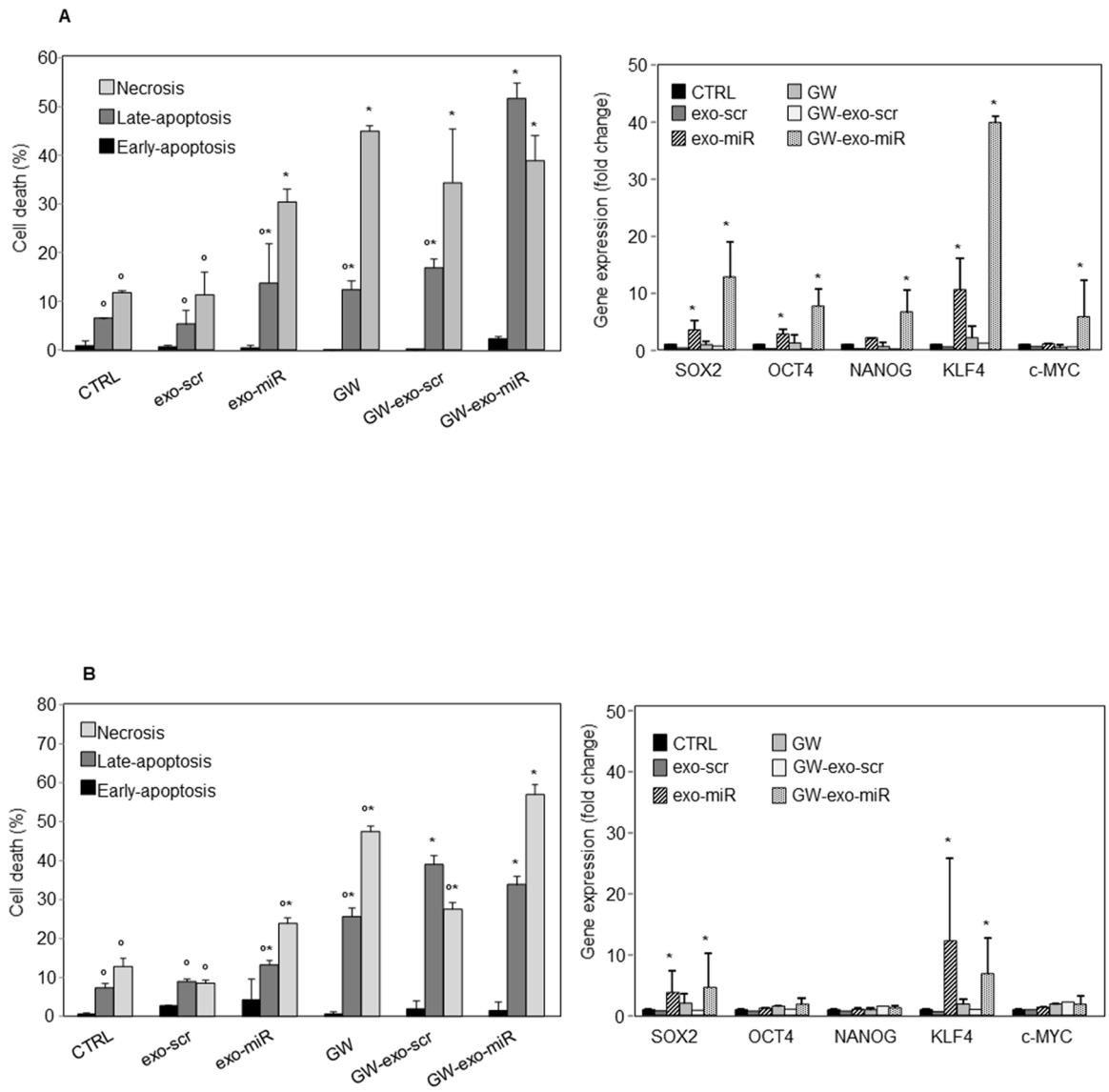

Fig. 3. Cell death and stemness in spheroids after combined treatments. Spheroids from MSTO-211H (**A**) and MPP89 (**B**) were treated with exosome scramble (exo-scr), miR-126-enriched exosome (exo-miR), GW4869 (GW), GW4869 plus exosome scramble (GW-exo-scr), and GW4869 plus miR-126-enriched exosome (GW-exo-miR) and the cell death and the expression of stemness genes (SOX2, OCT4, NANOG, KLF4, and c-MYC) were evaluated after 48 h and 24 h of drug exposure, respectively. Cell death was evaluated by annexin-V analysis and cells positive for annexin were in early apoptosis, those labelled both for annexin and PI were in late apoptosis and those positive for PI only died from necrosis. The results are mean values ± SD of three experiments performed in duplicate. Comparisons amongst groups were determined by one-way ANOVA with Tukey post-hoc analysis. The symbol '*' denotes statistically significant differences amongst untreated cells (CTRL) and treated cells; the symbol '°' denotes significant differences amongst the combined treatment (GW-exo-miR) and treated cells, $p < 0.05$.

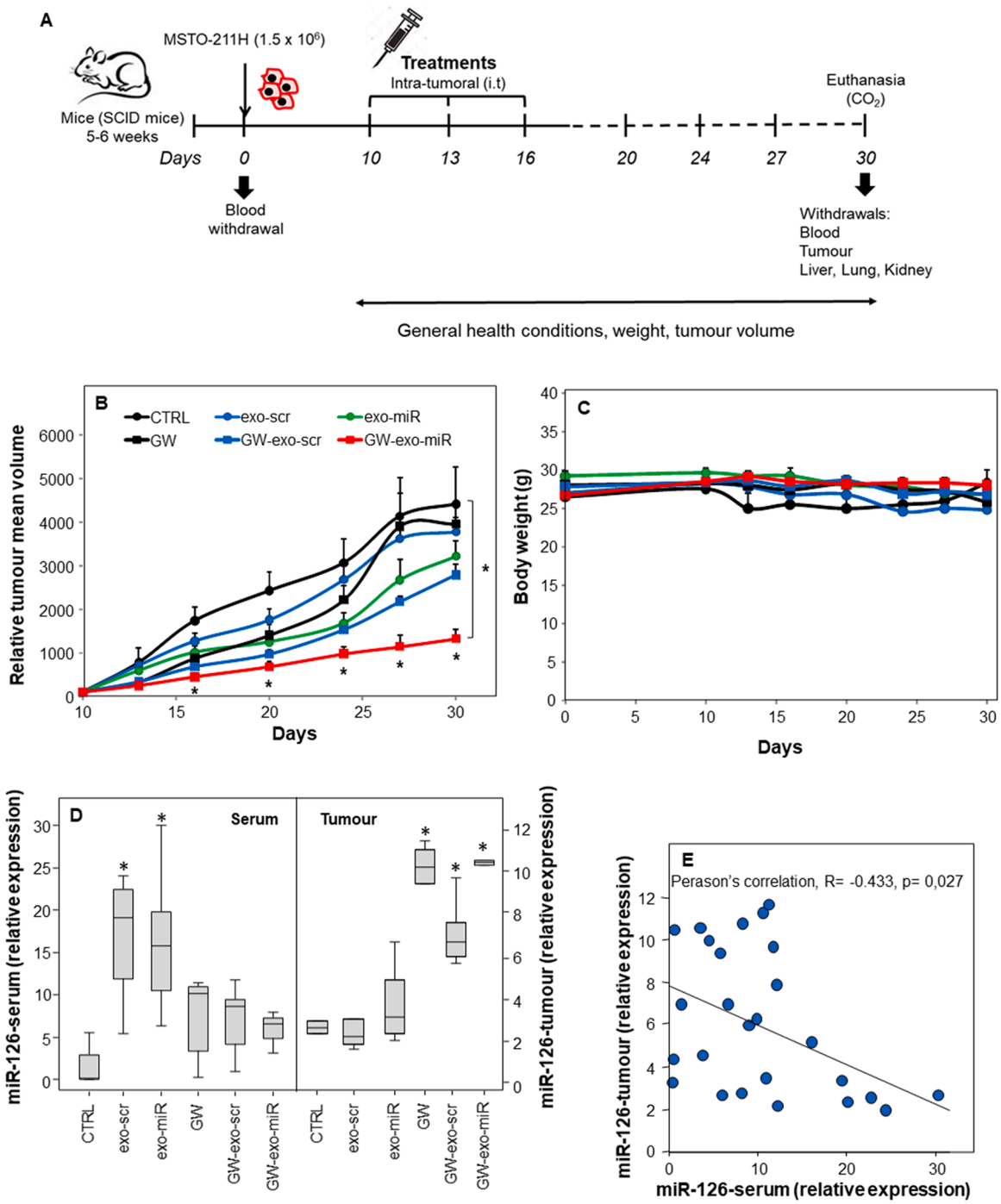

Fig. 4. Tumour growth in xenograft mice model. (**A**) Scheme of the in vivo experimental design. At day 0 NSG (NOD *scid* gamma) mice were inoculated with MSTO-211H cells and at day 10, 13 and 16 mice were treated with: PBS (control group, CTRL, $n = 8$), exosome scramble (exo-scr group, 0.7 mg/Kg, $n = 10$), miR-126-enriched exosome (exo-miR group, 0.7 mg/Kg, $n = 10$), GW4869 (GW group, 1 mg/Kg, $n = 10$), GW4869 plus exosome scramble (GW-exo-scr group, $n = 10$), and GW4869 plus miR-126-enriched exosome (GW-exo-miR group, $n = 10$). For the quantification of miR-126 in serum, peripheral blood was collected on days 0 and 30. On day 30 mice were sacrificed and tumour, lung, liver and kidney were harvested and analysed. **B**) Kinetic of tumour growth in control and treated groups. **C**) Time-course of mice weight from day 0 to day 30. **D**) Relative expression of miR-126 in serum (left side of the graph) and tumours (right side of the graph) at day 30. **E**) Correlation between miR-126 level in serum and tissue. Data of tumour volume are mean ± SEM. Comparisons amongst groups were determined by one-way ANOVA with Tukey post-hoc analysis. The kinetics of tumour growth were or was compared by the ANOVA repeated measure with Tukey's post hoc analysis. The symbol '*' denotes statistically significant differences amongst mice control group (CTRL) and treated mice, $p < 0.05$.

combination at day 24 but was lost at prolonged time. The growth rate of exo-miR and GW plus exo-scr tended to accelerate in the later period, resulting in the bigger tumour volume than that of GW plus exo-miR, even though not significant (Fig. 4**B**).

Of note, the treatments did not affect the body weight of the mice (Fig. 4**C**). Next, detection of miR-126 was performed to examine the expression of miR-126 both in serum and tumour tissue. The results showed that the treatment with exo-scr and exo-miR increased the level of circulating miR-126 compared with the control group (Fig. 4**D-left panel**). The miR-126 was sequestered in the tumour tissues by GW

treatment (Fig. 4**D-right panel**). A negative correlation was found between miR-126 content in tissue and miR-126 level in circulation (Fig. 4**E**).

Accumulation of miR-126 inhibited its gene targets such as SOX2, and the angiogenetic regulators VEGF1 and EGFL7 (Fig. 5**A**). A significant reduction of IL-6 expression was found in tumour treated with exo-scr and exo-miR, while no changes were observed for IL-1 (Fig. 5**B**).

Immunohistochemical staining experiments were performed to evaluate cell proliferation (Ki67) and angiogenesis (VEGF and CD31) in tumour tissue. As shown in Fig. 5**C, D**, the Ki67-positive cells, as well the expression of VEGF, were markedly reduced in the GW4869 plus exo-miR treated tumours. Even though the number of vessels was similar amongst the groups, a significant reduction in their size was found in tumours treated with exo-miR and to a greater extent in GW-exo-scr and GW-exo-miR groups, as reported in Fig. 5**D**. No sign of adverse effects was found in liver, lung and kidney tissues (Fig. 5**E**).

GW4869 treatment increases exo-miR-induced cell death by inhibiting autophagy

It has been reported that CSCs use autophagy to reinforce their resilience against microenvironmental stress conditions, such as starvation and hypoxia, promoting their survival to preserve their stemness phenotype [15]. In view of this, we evaluated the effect of the treatments on autophagy. As shown in Fig. 6**A, B,** the exo-scr and exo-miR treatment induced the expression of mTOR and its downstream substrate p70S6K in both MSTO-211H and MPP89 cells, which was associated with the inhibition of LC3I/LC3II expression. The mTOR activation and the reduced LC3I/LC3II expression were further increased when combined with the GW4869 (Fig. 6**C, D**). This scenario was previously observed in miR-126 transfected MPM cells as a result of increased autophagic flux [4], which was associated with AMPK-ULK1$^{ser-555}$ pathway activation (Fig. 6**E**). Next, the miR-126-induced autophagy was confirmed by morphological analysis; autophagosome formation was increased in exo-miR treated cells with respect to untreated cells. Conversely, autophagosomes were completely inhibited by GW4869, and when GW4869 was combined with exo-miR, the undigested materials including damaged organelles accumulated within the cells leading to cell death (Fig. 6**F**).

GW4869 and exo-miR combination induced necroptosis by PARP1 activation

To investigate the mechanism(s) involved in cell death induced by the combination GW4869 with exo-miR126, we evaluated the role of pro-apoptotic factors, such as PARP-1, BID and BAX, caspases activation and cytochrome-c (cyt-c) and apoptotic inducing factor (AIF) release from mitochondria into the cytoplasm. PARP-1 over-expression was found in GW4869 treated spheroids, which was further increased when GW4869 was combined with exo-scr and exo-miR, while no caspase activation was found (Fig. 7**A**). The PARP-1 activation was associated with mitochondrial permeabilization; the release of cyt-c and AIF from mitochondria to cytoplasm was observed after GW4869 plus exo-miR treatment (Fig. 7**B**). The densitometric analysis of the bands is reported in Fig. 7**C, D**. To determine the direct relationship between GW4869 plus exo-miR-induced necroptosis and PARP-1 induced by the combinatorial treatment, MPM-stem cell like were pre-treated with the 3-ABA, which efficiently inhibited PARP-1 activity. The inhibition of PARP-1 was associated with an abrogation of drugs-induced late apoptosis without affecting the percentage of necrotic cells (Fig. 7**E**).

Discussion

To date, there is no established treatment for recurrence of MPM after the multimodality approach. In the present study, we tested a miRNA-based therapy consisting in the combination of the miR-126 delivered via exosome with an inhibitor of exosome release. Exosomes have been proposed as natural nanoparticles for the successful delivery of miRNA into cells [16, 17], and exosome from endothelial cells are endogenously rich in miR-126; therefore, used as a vector.

Tumour-derived spheroids, which recapitulate features of naturally occurring tumours such as cellular phenotype, heterogeneity, drug response, and overall complexity, have been used as a model of MPM-stem cell like [18]. The MPM cells demonstrated different spheroid formation in vitro and exhibited different stemness features, reflecting the intra-tumour and interpatient heterogeneity. MiR-126-enriched exosomes (exo-miR) entered MPM-derived spheroids efficiently, increased their stemness phenotype and induced cytotoxicity (***cf Fig. 1***). However, at a prolonged time, the up taken miR-126 was released by the cells themselves using their exosomal system, thus limiting the miR-126-induced tumour suppressor property (***cf Fig. S1***). This suggests there may be a mechanism involved in the sorting process of miR-126 into exosomes derived from exo-miR treated MPM cells. This phenomenon was previously reported showing that all components of the 'stroma' took up exo-miR and released exosomes enriched in miR-126 into the microenvironment [9]. The secretion of tumour suppressor miRNAs has been found in cancers, including MPM [19, 20]. It was found that MPM tumour cells secreted significantly higher levels of miR-16–5p, compared to non-cancer mesothelial cells in exosomes. The block of exosome release using GW4869 led to significant reductions in exosomal miR-16–5p and significantly increased stores of cell cytoplasmic miR-16–5p [20]. Accordantly, to enhance the miR-126-induced anticancer effect, the exosome release inhibitor GW4869 was used [21]. Pre-incubating the MPM-stem cell like with GW4869 followed by exo-miR-126 treatment resulted in miR-126 accumulation within the cells and subsequent massive cell death.

The MPM-stem cell like were more sensitive to the GW4869 and exo-miR-126 combination with respect to their adherent counterparts (***cf Fig. 3 and Fig. S2***), and the stemness phenotype increased the effect of the combined treatment (***cf Fig. 3***). The anticancer effect of GW4869 and exo-miR-126 combination was confirmed in vivo by the xenograft SCID mice model (***cf Fig. 4***). Mice treated with the drug combination inhibited the tumour growth significantly without affecting body weight. Tumour growth inhibition was also observed in mice treated either with exo-miR or GW4869 plus exo-scr; we can postulate that exo-miR with high miR-126 content transfer comparable amount of miR-126 into cancer tissue of exo-scr (low miR-126 content) when combined with the exosome release inhibitor (***cf Fig. 4E-right panel***). Notably, the exo-miR and exo-scr treatment increased the level of miR-126 into circulation, which was [1–29] sequestered by the cancer tissue after GW4869 treatment. Although the level of miR-126 in GW4869-treated tumours was comparable to that found in tumour treated with the GW and exo-miR combination (*cf Fig. 4D*), the accumulation of miR-126 in cancer treated with the combination resulted in the inhibition of cell proliferation, angiogenesis, and loss of malignancy. Notably, the accumulation of miR-126 within the tumours markedly reduced the vessel blood size as a sign of non-malignancy (***cf Fig. 5***). As previously reported normalization of tumour vasculature prevents cancer cell intravasation [22]. We can hypothesize that the GW treatment blocked the release of endogenous miRNA through the exosomes, thus resulting in intracellular miRNA accumulation, including the miR-126. When the GW was combined with exo-miR a further increase of miR-126 level in tumours may occur, thus resulting in tumour growth arrest. However, the increased miR-126 may be found only within a few days from the last treatment. At a prolonged time, 14 days from the last treatment, the miR-126 within tumour may undergo to a rearrangement, thus reaching a steady state level of miR-126 comparable to that found in tumours treated with the GW4869 only.

Autophagy is involved in these processes (***cf Fig. 6***). As previously observed [4, 5], miR-126 induced autophagosome formation associated with mTOR-AMPK-ULK1$^{ser-555}$ pathway activation. On the other hand, GW4869 inhibited autophagy; GW4869 is a potent inhibitor of

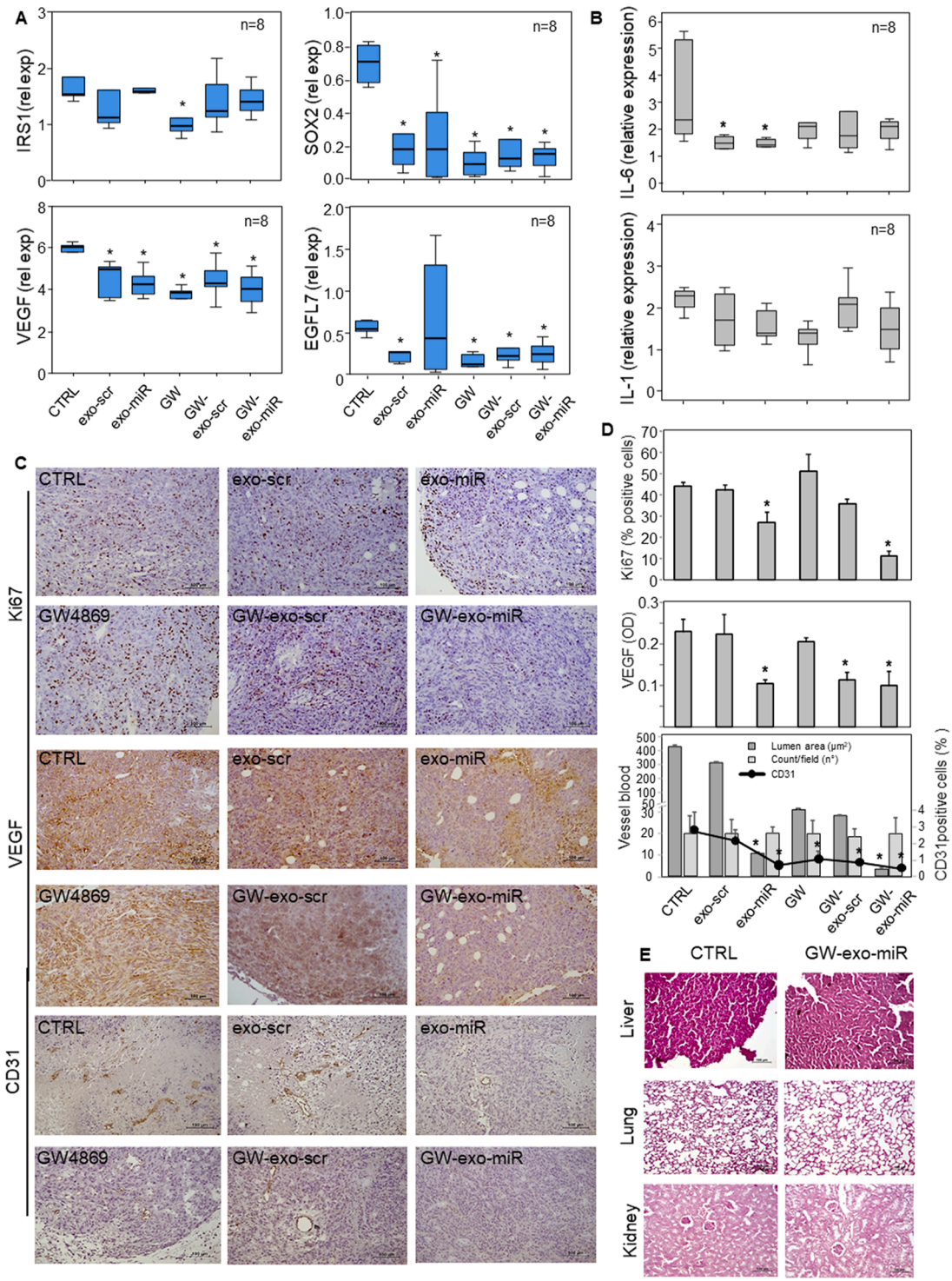

Fig. 5. MiR-126 targets, cell proliferation and angiogenesis in mice tumours. Tumour tissues from MSTO-211H tumour-bearing mice, before (CTRL) and after treatments (exo-scr, exo-miR, GW4869, GW-exo-scr, GW-exo-miR), were evaluated for the expression of miR-126 targets (IRS1, SOX2, VEGF and EGFL7) (**A**), and inflammatory cytokines (IL-6 and IL-1) (**B**). Immunohistochemical (IHC) analysis of Ki67, VEGF, and CD31 in tumour tissues of mice (**C**). The level of Ki67 and VEGF was expressed as the percentage of positive cells and optical density (OD), respectively; the vessel blood was evaluated as vessel number, CD31-positive cells, and lumen area (**D**). The quantification was performed by using ImageJ software. Haematoxylin and eosin (H&E) staining of liver, lung, and kidney of mice tissues (**E**). The images are representative of three independent experiments and the data shown are mean values ± SD. Scale bar=100 µm. Comparisons amongst groups were determined by one-way ANOVA with Tukey post-hoc analysis. The symbol '*' denotes statistically significant differences amongst mice control group (CTRL) and treated mice, $p < 0.05$.

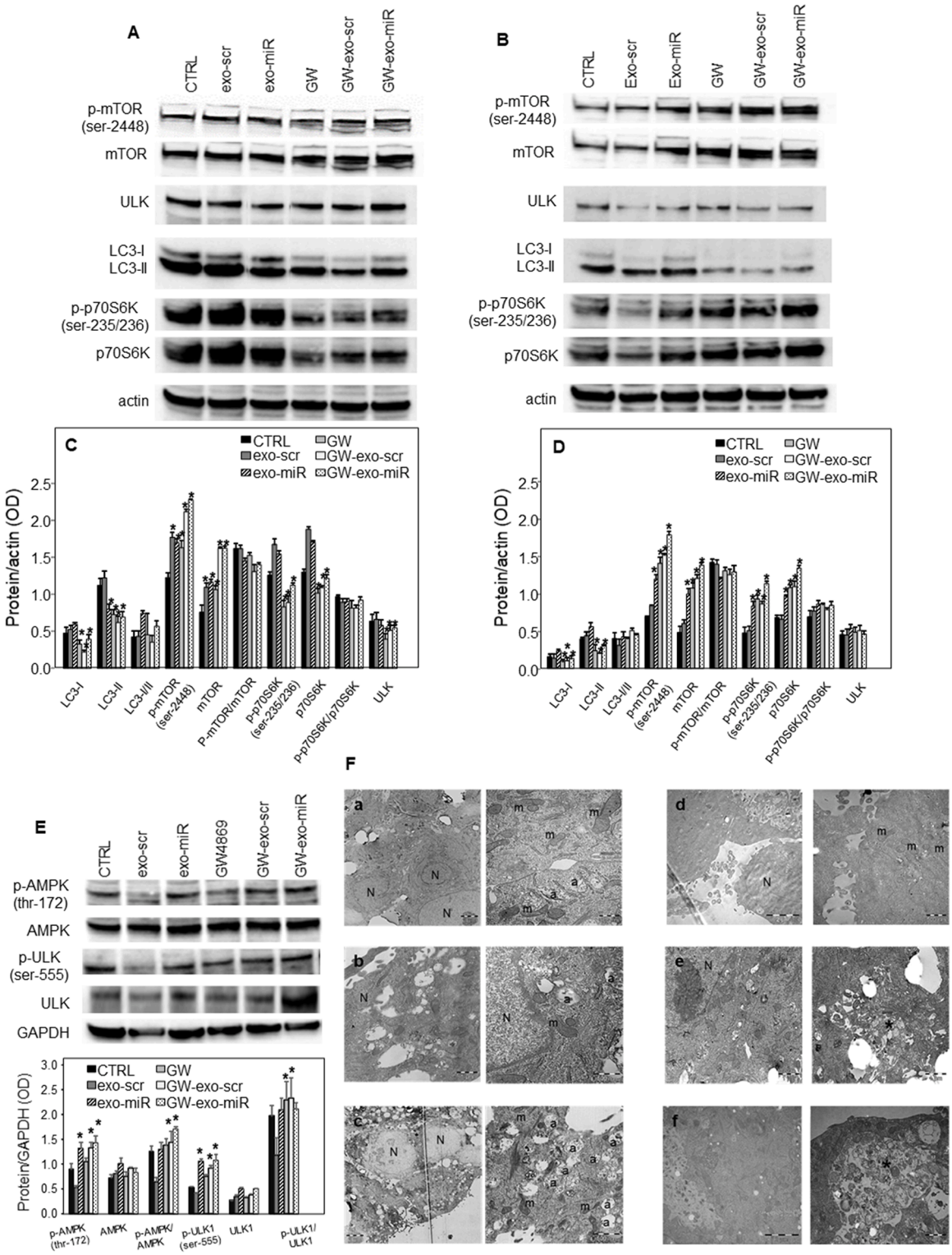

Fig. 6. Autophagy pathway in spheroids. Spheroids from MSTO-211H (**A**) and MPP89 (**B**), before (CTRL) and after treatments (exo-scr, exo-miR, GW4869, GW-exo-scr, GW-exo-miR), were analysed for relative protein levels of p-mTOR$^{ser-2448}$, mTOR, ULK, LC3I/II and p-p70S6K$^{ser-235/236}$, p70S6K. Densitometric evaluation of the bands shown relative to actin in MSTO-211H (**C**) and MPP89 (**D**) cancer stem cell-like. **E**) Spheroids from MSTO-211H before (CTRL) and after treatments, were analysed for relative protein levels of pAMPK$^{thr-172}$, AMPK, pULK1$^{ser-555}$ and ULK1 and band densitometry evaluated. **F**) Transmission electron microscopy (TEM) analysis of spheroids from MSTO-211H untreated (a) or treated with exo-scr (b), exo-miR (c), GW4869 (d), GW-exo-scr (e) and GW-exo-miR (f). N = nucleus, m = mitochondria, a = autophagosomes. The images are representative of three independent experiments and the data shown are mean values ± SD. Comparisons amongst groups were determined by one-way ANOVA with Tukey post-hoc analysis. The symbol '*' denotes statistically significant differences amongst control group (CTRL) and treated cells, $p < 0.05$.

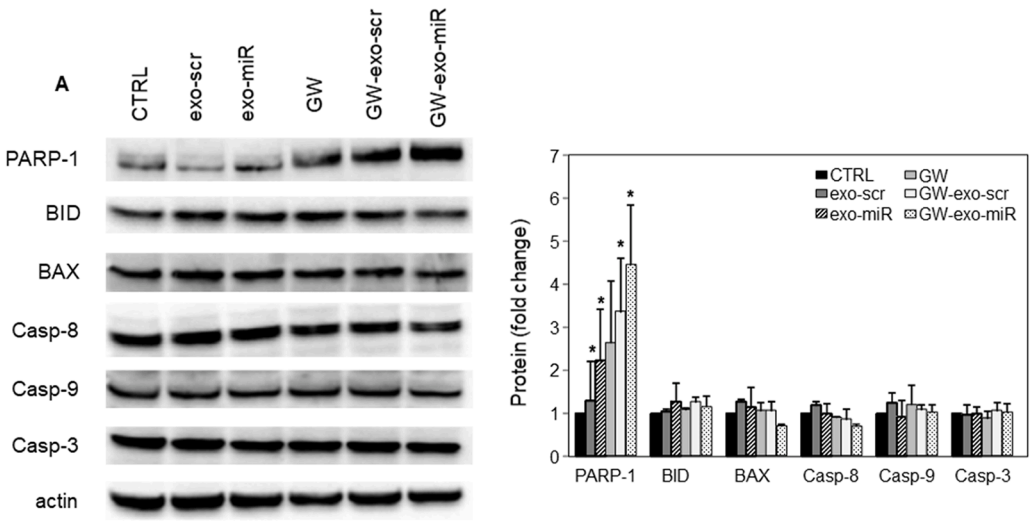

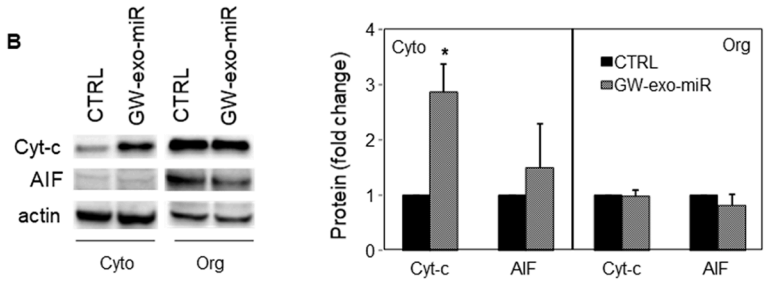

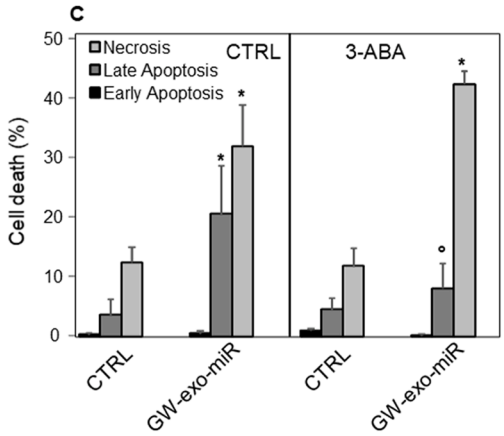

Fig. 7. Cell death pathway in spheroids. Spheroids from MSTO-211H before (CTRL) and after treatments (exo-scr, exo-miR, GW4869, GW-exo-scr, GW-exo-miR), were analysed for relative levels of PARP-1, BID, BAX, Caspase-8, Caspase-9, Caspase-3 (**A**). Cell fractionation, cytoplasm (cyto) and organelle (org) fraction, was performed to evaluate the cytochrome-c (cyt-c) and AIF release from organelles, including mitochondria, into the cytoplasm (**B**). The presence of cyt-c and AIF in the org fraction but not in the cytoplasm fraction of non-treated cells (CTRL) confirm the purity of cell fractions. The densitometry evaluation of the bands relative to actin are shown in the graphs on the right. Cytotoxic effect of the combinatorial treatment on spheroids in the absence or presence of 3-ABA after 48 h of drug exposure (**C**). The images are representative of three independent experiments and the data shown are mean values ± SD. Comparisons amongst groups were determined by one-way ANOVA with Tukey post-hoc analysis. The symbol '*' denotes statistically significant differences amongst control (CTRL) and treated cells; The symbol '°' denotes statistically significant differences between control (CTRL) and 3-ABA treated cells, $p < 0.05$.

sphingomyelinase (SMase), a key enzyme that mediates stress-induced autophagic flux [23, 24]. Therefore, we can hypothesize that the protective function of autophagy in response to stress stimuli, acts as a protective mechanism to ensure cell survival, and if the cells cannot restore the damage, they will die.

Necroptosis was the type of cell death induced by force-feeding the MPM-derived spheroids with miR-126. The GW4869 and exo-miR treatment induced cell death associated with poly (ADP-ribose) polymerase-1 (PARP-1) induction (***cf Fig. 7***). PARP-1 over-activation provokes ATP depletion and consequent autophagy pathway activation through the AMPK-mTOR pathway to ensure cell survival. Autophagy inhibition during low cell energy availability could generate a metabolic crisis that promotes necroptosis activation. Several studies highlight the caspase interaction as crucial in the regulation of the autophagy pathway and the interplay between autophagy, necrosis, and apoptosis [25]. PARP1 activation generates the PAR polymer in the nucleus and it translocates to mitochondria to mediate cyt-c and AIF release. Subsequently, AIF protein translocated from the cytoplasm to the nucleus, resulting in the induction of chromatin condensation with ensuing cell death [26].

In conclusion, a novel approach of miRNA-based cancer therapy using an exosome release inhibitor (GW4869) has been proposed. The

GW4869 combined with exo-miR induced death in CSCs and inhibited tumour growth by inducing three sequential events: intracellular miR-126 accumulation, which in turn induced a protective autophagy that was inhibited by GW4869. This therapeutic approach was registered as 'high efficacy oncological therapy based on miRNA', patent n 102,021,000,010,001.

Concerning the above-mentioned possible therapeutic tools in miRNA delivery, it might be tempting to consider exosomes as a potential therapeutic tool in the handling of MPM. Even though there are potential opportunities for miRNA-enriched exosomes to kill cancer cells, there are some limitations, which include miRNA-loading and efficiency of mass production of exosomes. A standardized protocol for large-scale production and isolation of clinical-grade exosomes is still lacking. As well, the choice of donor cells as the source of exosomes has not been fully clarified [27–29]. Therefore, further studies are required to develop appropriate protocols for miRNA-enriched exosomes.

Authors' contributions

Federica Monaco: Conceptualization, investigation; Laura De Conti, Simone Vodret, Nunzia Zanotta, Manola Comar, Laura Graciotti, Gianluca Fulgenzi, Sandra Manzotti and Corrado Rubini: methodology, formal analysis; Massimo Bovenzi: Supervision, resources, funding acquisition. Marco Baralle: Supervision, writing-original draft and editing. Marco Tomasetti: Conceptualization, investigation, data curation, writing-original draft. Lory Santarelli: supervision, resources. All authors read and approved the final manuscript.

Supplementary material

Figure S1
Figure S2
Supplementary-Materials.pdf

CRediT authorship contribution statement

Federica Monaco: Conceptualization, Investigation. **Laura De Conti:** Methodology, Formal analysis. **Simone Vodret:** Methodology, Formal analysis. **Nunzia Zanotta:** Methodology, Formal analysis. **Manola Comar:** Methodology, Formal analysis. **Sandra Manzotti:** Methodology, Formal analysis. **Corrado Rubini:** Methodology, Formal analysis. **Laura Graciotti:** Methodology, Formal analysis. **Gianluca Fulgenzi:** Methodology, Formal analysis. **Massimo Bovenzi:** Supervision, Resources, Funding acquisition. **Marco Baralle:** Supervision, Writing – original draft. **Marco Tomasetti:** Conceptualization, Investigation, Data curation, Writing – original draft. **Lory Santarelli:** Supervision, Resources.

Declaration of Competing Interest

The authors declare that they have no competing interests.

Acknowledgments

This work was supported by a grant from Region Friuli Venezia Giulia - Central Directorate for Health, Social Policies and Disability (Italy), Protocol n. 0016902/P (11/09/2018), Decree n. 1463/SPS (05/10/2018).

Supplementary materials

Supplementary material associated with this article can be found, in the online version, at doi:10.1016/j.tranon.2022.101400.

References

[1] R. Asciak, V. George, N.M. Rahman, Update on biology and management of mesothelioma, Eur. Respir. Rev. 30 (2021), 200226.
[2] F. Larose, N. Quigley, Y. Lacasse, S. Martel, L. Lang-Lazdunski, Malignant pleural mesothelioma: comparison of surgery-based trimodality therapy to medical therapy at two tertiary academic institutions, Lung Cancer 156 (2021) 151–156.
[3] M. Tomasetti, S. Staffolani, L. Nocchi, J. Neuzil, E. Strafella, N. Manzella, et al., Clinical significance of circulating miR-126 quantification in malignant mesothelioma patients, Clin. Biochem. 45 (2012) 575–581.
[4] M. Tomasetti, F. Monaco, N. Manzella, J. Rohlena, K. Rohlenova, S. Staffolani, et al., MicroRNA-126 induces autophagy by altering cell metabolism in malignant mesothelioma, Oncotarget 7 (2016) 36338–36352.
[5] M. Tomasetti, L. Nocchi, S. Staffolani, N. Manzella, M. Amati, J. Goodwin, et al., MicroRNA-126 suppresses mesothelioma malignancy by targeting IRS1 and interfering with the mitochondrial function, Antioxid. Redox Signal. 21 (2014) 2109–2125.
[6] I. Dasgupta, A. Chatterjee, Recent Advances in miRNA Delivery Systems, Methods Protoc 4 (2021) 10.
[7] Z. Mirza, S. Karim, Nanoparticles-based drug delivery and gene therapy for breast cancer: recent advancements and future challenges, Semin. Canc. Biol. 69 (2021) 226–237.
[8] M.I. Elewaily, A.R. Elsergany, Emerging role of exosomes and exosomal microRNA in cancer: pathophysiology and clinical potential, J. Cancer Res. Clin. Oncol. 147 (2021) 637–648.
[9] F. Monaco, S. Gaetani, F. Alessandrini, A. Tagliabracci, M. Bracci, M. Valentino, et al., Exosomal transfer of miR-126 promotes the anti-tumour response in malignant mesothelioma: role of miR-126 in cancer-stroma communication, Cancer Lett 463 (2019) 27–36.
[10] H. Duan, Y. Liu, Z. Gao, W. Huang, Recent advances in drug delivery systems for targeting cancer stem cells, Acta Pharm. Sin. B 11 (2021) 55–70.
[11] A. Bellini, A. Dell'Amore, S. Terzi, G. Zambello, A. Zuin, G. Pasello, et al., Relapse Patterns and Tailored Treatment Strategies for Malignant Pleural Mesothelioma Recurrence after Multimodality Therapy, J. Clin. Med. 10 (2021) 1134.
[12] Y.K. Ho, W.T. Xu, H.P. Too, Direct quantification of mRNA and miRNA from cell lysates using reverse transcription real time PCR: a multidimensional analysis of the performance of reagents and workflows, PLoS ONE 8 (2013) e72463.
[13] S. Asaga, C. Kuo, T. Nguyen, M. Terpenning, A.E. Giuliano, D.S. Hoon, Direct serum assay for microRNA-21 concentrations in early and advanced breast cancer, Clin. Chem. 57 (2011) 84–91.
[14] A. Faustino-Rocha, P.A. Oliveira, J. Pinho-Oliveira, C. Teixeira-Guedes, R. Soares-Maia, R.G. da Costa, et al., Estimation of rat mammary tumor volume using caliper and ultrasonography measurements, Lab. Anim. 42 (2013) 217–224.
[15] M. Najafi, K. Mortezaee, J. Majidpoor, Cancer stem cell (CSC) resistance drivers, Life Sci 234 (2019), 116781.
[16] T. Li, L. Zhu, L. Zhu, P. Wang, W. Xu, J. Huang, Recent Developments in Delivery of MicroRNAs Utilizing Nanosystems for Metabolic Syndrome Therapy, Int. J. Mol. Sci. 22 (2021) 7855.
[17] B. Roy, S. Ghose, S. Biswas, Therapeutic strategies for miRNA delivery to reduce hepatocellular carcinoma, Semin. Cell Dev. Biol. S1084-9521 (21) (2021), 00079-3.
[18] C. Blanquart, M.C. Jaurand, D. Jean, The Biology of Malignant Mesothelioma and the Relevance of Preclinical Models, Front. Oncol. 10 (2020) 388.
[19] P. Kanlikilicer, M.H. Rashed, R. Bayraktar, R. Mitra, C. Ivan, B. Aslan, et al., Ubiquitous Release of Exosomal Tumor Suppressor miR-6126 from Ovarian Cancer Cells, Cancer Res 76 (2016) 7194–7207.
[20] P.B. Munson, E.M. Hall, N.H. Farina, H.I. Pass, A. Shukla, Exosomal miR-16-5p as a target for malignant mesothelioma, Sci. Rep. 9 (2019) 11688.
[21] M. Catalano, L. O'Driscoll, Inhibiting extracellular vesicles formation and release: a review of EV inhibitors, J. Extracell. Vesicles 9 (2019), 1703244.
[22] B. He, A. Johansson-Percival, J. Backhouse, J. Li, G.Y.F. Lee, J. Hamzah, et al., Remodeling of Metastatic Vasculature Reduces Lung Colonization and Sensitizes Overt Metastases to Immunotherapy, Cell Rep 30 (2020) 714–724.
[23] C. Perrotta, D. Cervia, C. De Palma, E. Assi, P. Pellegrino, M.T. Bassi, et al., The emerging role of acid sphingomyelinase in autophagy, Apoptosis 20 (2015) 635–644.
[24] M.J. Back, H.C. Ha, Z. Fu, J.M. Choi, Y. Piao, J.H. Won, et al., Activation of neutral sphingomyelinase 2 by starvation induces cell-protective autophagy via an increase in Golgi-localized ceramide, Cell Death Dis 9 (2018) 670.
[25] Y. Gong, Z. Fan, G. Luo, C. Yang, Q. Huang, K. Fan, et al., The role of necroptosis in cancer biology and therapy, Mol. Cancer 18 (2019) 100.
[26] M. Mashimo, M. Onishi, A. Uno, A. Tanimichi, A. Nobeyama, M. Mori, et al., The 89-kDa PARP1 cleavage fragment serves as a cytoplasmic PAR carrier to induce AIF-mediated apoptosis, J. Biol. Chem. 296 (2021), 100046.
[27] Y.S. Chen, E.Y. Lin, T.W. Chiou, H.J. Harn, Exosomes in clinical trial and their production in compliance with good manufacturing practice, Ci Ji Yi Xue Za Zhi 32 (2019) 113–120.
[28] M. Mendt, S. Kamerkar, H. Sugimoto, K.M. McAndrews, C.C. Wu, M. Gagea, et al., Generation and testing of clinical-grade exosomes for pancreatic cancer, JCI Insight 3 (2018) e99263.
[29] D. Bellavia, L. Raimondi, V. Costa, A. De Luca, V. Carina, M. Maglio, et al., Engineered exosomes: a new promise for the management of musculoskeletal diseases, Biochim. Biophys. Acta Gen. Subj. 1862 (2018) 1893–1901.